International Journal of Civil Engineering

Seismic Geotechnique

Study of the behavior of pile groups during lateral spreading in medium dense sands by large scale shake table test

A. Kavand[1], S. M. Haeri[2,*], A. Asefzadeh[3], I. Rahmani[4], A. Ghalandarzadeh[5], A. Bakhshi[6]

Received: May 2013, Revised: October 2013, Accepted: December 2013

Abstract

In this paper, different aspects of the behavior of 2×2 pile groups under liquefaction-induced lateral spreading in a 3-layer soil profile is investigated using large scale 1g shake table test. Different parameters of the response of soil and piles including time-histories of accelerations, pore water pressures, displacements and bending moments are presented and discussed in the paper. In addition, distribution of lateral forces due to lateral spreading on individual piles of the groups is investigated in detail. The results show that total lateral forces on the piles are influenced by the shadow effect as well as the superstructure mass attached to the pile cap. It was also found that lateral forces exerted on the piles in the lower half of the liquefied layer are significantly larger than those recommended by the design code. Based on the numerical analyses performed, it is shown that the displacement based method is more capable of predicting the pile group behavior in this experiment comparing to the force based method, provided that the model parameters are tuned.

Keywords: *Liquefaction, Lateral spreading, 1g shake table test, Pile group, Lateral soil pressure, p-y curves, Numerical analysis.*

1. Introduction

Several important structures supported on pile foundations have been severely damaged due to liquefaction during past destructive earthquakes around the world. These damages have been reported to be more extensive in areas located in mildly sloping grounds or waterfronts where lateral spreading has occurred. Numerous examples have been documented in the literature in this regard, among which the 1964 Niigata, Japan, the 1989 Loma Prieta, USA, the 1995 Kobe, Japan and the 2010 Haiti earthquakes are the most well-known ones [1-6].

** Corresponding author: smhaeri@sharif.edu*
1 Assistant Professor, Geotechnical Engineering, School of Civil Engineering, College of Engineering, University of Tehran, Tehran, Iran
2 Professor, Geotechnical Engineering, Department of Civil Engineering, Sharif University of Technology, Tehran, Iran
3 PhD Candidate, Geotechnical Engineering, Department of Civil and Environmental Engineering, University of Maryland, USA
4 Assistant Professor, Geotechnical Engineering, Marine Transportation & Technology Division, Transportation Research Institute, Tehran, Iran
5 Associate Professor, Geotechnical Engineering, School of Civil Engineering, College of Engineering, University of Tehran, Tehran, Iran
6 Assistant Professor, Earthquake Engineering, Department of Civil Engineering, Sharif University of Technology, Tehran, Iran

Liquefaction-induced lateral spreading is referred to as the lateral displacement of a gently sloping ground (0.3% to 5% slope) or a level ground ending in a free face as a result of liquefaction in shallow underlying saturated loose cohesionless deposits during an earthquake.

Horizontal displacements in a lateral spreading can be up to several meters which can impose significant kinematic lateral forces to pile foundations resulting in extensive damages. Damages will be more severe in cases where a non-liquefiable crust layer (e.g. the soil above the water level) exists on top of a liquefiable layer since the crust layer can ride on top of the spreading liquefied soil exerting substantial lateral pressure on the pile foundations. Damages to pile groups in past earthquakes were observed to be mostly localized in three distinct locations along the piles i.e. the connection between pile and cap, the boundary between liquefiable layer and non-liquefiable crust layer and the boundary between liquefiable layer and base non-liquefiable layer [1,7,8].

Geotechnical physical models can be used as a useful tool for understanding the mechanisms of soil-pile interaction in laterally spreading ground. In this regard, response of pile foundations under lateral spreading has been experimentally investigated by different researchers during previous studies implementing 1g shake table [9-18] or Ng centrifuge [7,19-23] physical model tests and field experiments [24]. Basic mechanisms of pile response under lateral spreading have been scrutinized in these studies and the effects of different parameters on the pile response have been evaluated including presence of a non-

liquefiable crust layer, thickness of liquefiable layer, permeability of liquefiable soil, group size (number of piles and pile spacing), stiffness of the pile group and geometry of ground surface (being located in sloping ground or behind waterfront structures). Indeed, findings from previous studies have effectively improved the understanding of pile behavior in laterally spreading ground, yet the complexity of the problem, some aspects of the soil-pile interaction in laterally spreading ground have not been fully identified. Therefore, the problem has still remained an issue of research in geotechnical earthquake engineering.

This paper aims to study the behavior of 2×2 pile groups embedded in a 3-layer soil profile consisting of a base non-liquefiable layer, a middle liquefiable layer and an upper non-liquefiable layer, by conducting 1g large scale shake table test. A lumped mass was attached to one of the pile groups to investigate the effects of superstructure on the pile response during lateral spreading. Distribution of lateral forces among the individual piles of the groups is also focused on, obtaining contribution coefficients of lateral forces for different pile rows of the groups. Exerted lateral forces due to lateral spreading on piles are also compared to current recommendations for design of pile groups against lateral spreading. Experimental p-y curves are back-calculated from the recorded data to understand the interaction of pile groups with laterally spreading soil. Finally, on the basis of the test results, numerical models are calibrated and analyzed to predict the behavior of pile groups under lateral spreading during the experiment.

2. 1g Shaking Table Test

The shake table test was carried out by using shake table facility of the Earthquake Engineering Research Center at Sharif University of Technology (SUT) which is a 4m×4m, 3DOFS facility, capable of shaking a 500 kN payload in longitudinal direction and $2\times200\,kN$ payload in transversal direction both with a maximum base acceleration of $20\frac{m}{s^2}$ and a maximum frequency of 50Hz.

2.1. Physical model

The employed physical model consists of two separate 2×2 pile groups. A lumped mass of 12 kg was attached to the cap of one of the pile groups in order to study the effects of superstructure loads on pile response during lateral spreading.

The physical model was constructed and tested in a rigid box having 3.5m length, 1.0m width and 1.5m height. The box length was selected long enough to provide required space for the laterally spreading soil during its movement towards the downslope. In contrary to physical modeling of dynamic soil–pile interaction, rigid boundary condition in this study is of low degree of importance as the studied phenomenon is rather kinematic in nature. In order to monitor soil movement during lateral spreading, two large Plexiglas windows were provided in one of the longitudinal sidewalls of the rigid box. Schematic cross section and plan views of the physical model along with the general layout of transducers are shown in Fig. 1.

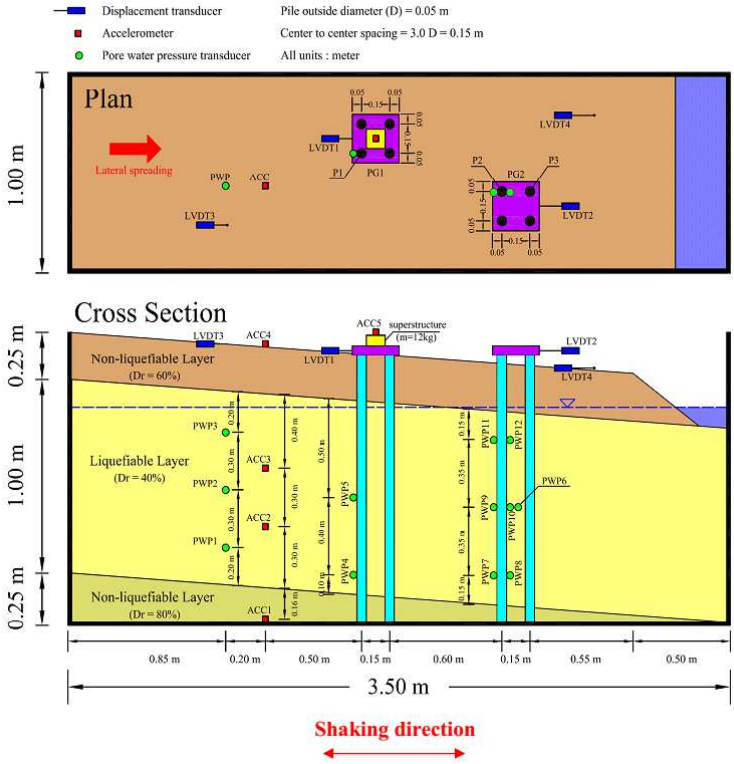

Fig. 1 Plan and cross section views of the physical model along with the locations of installed transducers

As seen in this figure, the model ground consists of a 3-layer soil profile sloping down by 4 degrees. The top layer is 0.25m thick consisting of medium dense sand having a relative density of about 60% which is located mostly above the water level. The middle layer is a 1m thick liquefiable sand layer with a relative density of about 40% and the lower layer is a non-liquefiable sand layer with a relative density of about 80%.

The liquefiable layer was constructed by water sedimentation technique and implementing a sand pluviator which was designed and constructed for raining sand in water under controlled conditions. The lower non-liquefiable layer was prepared by compaction of the wet sand while the top non-liquefiable layer was constructed by air pluviation, accompanied by a moderate compaction using a light hammer.

All model piles were constrained against translation and rotation at the bottom and were fixed in the pile cap at the top. The center-to-center distance between the piles of the groups was 3.0D (D is the outer diameter of pile). Top and side views of the physical model on SUT shake table device are shown in Fig. 2.

(a)

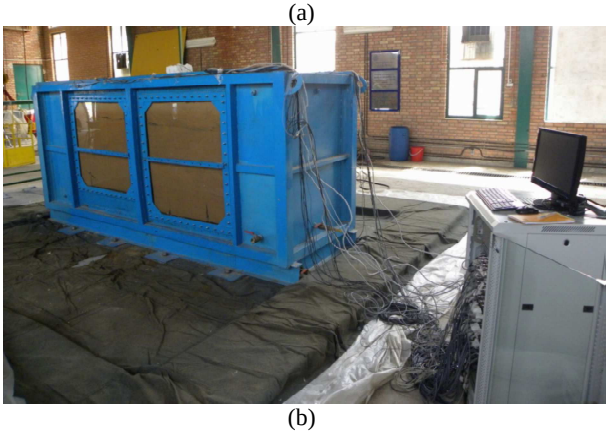

(b)

Fig. 2 Physical model on SUT shake table (a) top view, (b) side view

2.2. Material properties

All required material properties of the physical model were obtained using similitude law suggested by Iai et al. [25] and Iai [26]. Considering dimensions of the rigid box, a geometric scale of $\lambda = 8$ was selected for this purpose. The scaling factors used in this study are summarized in Table 1.

Table 1 Scaling factors for 1g shaking table test

Parameter	Scaling factors proposed by Iai et al. [25] (prototype/model)	Scaling factors in this study (prototype/model)
Length (l)	λ	8.0
Density (ρ)	λ_ρ	1.0
Strain (ε)	λ_ε	1.0
Time (t)	$(\lambda\lambda_\varepsilon)^{0.5}$	2.828
Frequency (f)	$(\lambda\lambda_\varepsilon)^{-0.5}$	0.353
Acceleration ($\ddot{u}$)	1.0	1.0
Displacement (u)	$\lambda\lambda_\varepsilon$	8.0
Stress (σ)	$\lambda\lambda_\rho$	8.0
EI of Pile	$\lambda^5\lambda_\rho / \lambda_\varepsilon$	32768

Firoozkuh silica sand No. 161, crushed sand with a uniform gradation, was used for construction of the soil layers in the experiment. A summary of the properties of Firoozkuh sand is presented in Table 2. As mentioned earlier, a target relative density of 40% was considered for the liquefiable layer in this study which is categorized in medium density range. Prototype pile foundations were designed based on Japan Road Association design code (JRA) [27] to withstand the exerted lateral spreading forces. Geometrical and mechanical properties of the model piles were subsequently obtained using the aforementioned similitude laws. All piles of the model were made of aluminum pipes (T6061 alloy) while pile caps were made of Plexiglas. Mechanical and geometrical characteristics of the model piles as well as the pile caps are summarized in Tables 3 and 4, respectively.

Table 2 Properties of Firoozkuh silica sand no.161

G_s	e_{max}	e_{min}	C_u	D_{50} (mm)	D_{10} (mm)	D_{90} (mm)
2.70	0.87	0.608	1.49	0.24	0.18	0.39

Table 3 Material characteristics of model piles

Material	Height (m)	Outer/inner diameter (cm)	I (cm^4)	EI ($kN.m^2$)
Aluminum	1.25	5.0/4.74	5.901	4.387

Table 4 Material characteristics of pile caps

Material	Dimensions (B×L×t)	Weight (kg)	E (kN/m^2)
Plexiglas	25cm×25cm×5cm	3.510	3.1×10^6

2.3. Instrumentation

As sketched in Fig. 1, the transducers used in this study include accelerometers in free field (far from the piles) and

on top of the pile caps to measure soil and pile cap accelerations respectively; pore pressure transducers in free field as well as close to the pile groups to precisely monitor generation and dissipation of excess pore water pressures; displacement transducers (LVDTs) attached to the pile caps and mounted in free field to record pile cap and soil lateral displacements respectively; and finally strain gauges attached to some individual piles of the groups to record bending moments in piles during lateral spreading. In addition, during the experiment digital camcorders and cameras were implemented both at top and side of the physical model to observe deformation patterns of soil and piles in horizontal and vertical views, respectively.

2.4. Base excitation

The physical model was shaken with a sinusoidal base acceleration having a frequency of 3.0 Hz and amplitude of 0.3g. Duration of the base excitation was 12.0 sec including two rising and falling parts, each of duration of about 1.0 sec at beginning and end of the shaking. Base shaking was applied in longitudinal direction, parallel to the model slope.

3. Summary of General Experimental Results

In this section, a summary of the main data measured during the test (in terms of model scale) is presented and discussed.

3.1. Soil acceleration records in free field

Time histories of soil acceleration in free field (soil far from the piles) at different depths of the model are plotted in Fig. 3. Positive amplitude in this figure corresponds to downslope direction. As observed, the amplitude of acceleration records in liquefiable layer descended significantly after a few cycles of shaking at the same time that the soil liquefied and consequently lost its shear strength. However, after liquefaction, acceleration recorded at the surface of non-liquefiable crust layer (ACC4) shows some amplification relative to the accelerations of deeper depths, in liquefied layer, which is due to the fact that the crust layer is not liquefiable. Also, it is clear that the acceleration amplified in the soil from the bottom towards the ground surface before the liquefaction and the amplification is greater in downslope direction. Minor spikes observed in soil acceleration records can be attributed to the momentary dilation of the liquefied soil.

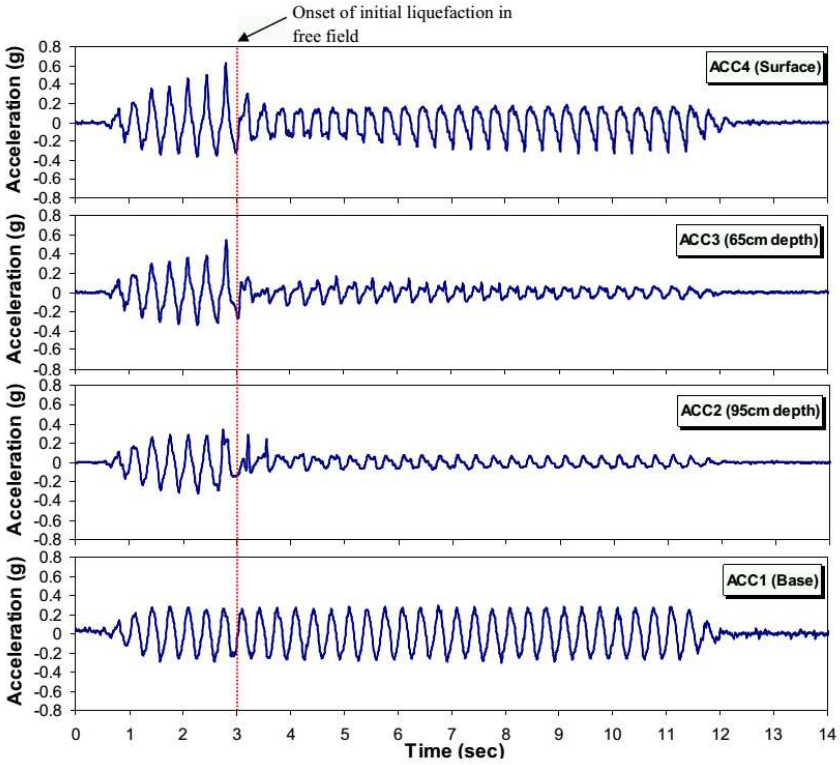

Fig. 3 Time histories of soil acceleration in free field

3.2. Excess pore water pressure records

Pore water pressures were recorded in different parts of the model including free field and areas close to the piles by installing pore water pressure (PWP) transducers. Representative excess pore water pressure records are shown in Fig. 4. Pore pressure transducers PWP1, PWP2 and PWP3 were located in free field while PWP7, PWP9 and PWP11 were installed adjacent to the upslope side of pile P2 and PWP6 was placed in the soil inside pile group PG2. General trends of recorded pore water pressures show that the soil in free field liquefied after about 7

cycles of shaking; and the upper the elevation, the sooner the indication of liquefaction. As expected, dissipation of excess pore water pressure or consolidation of liquefied soil started from the bottom of liquefiable layer and followed by reduction in excess pore pressure in upper elevations. Suction spikes in free field records during the time span that the soil is approaching liquefaction are also detectable, especially at shallow depths, indicating momentary dilation due to the soil movement towards downslope.

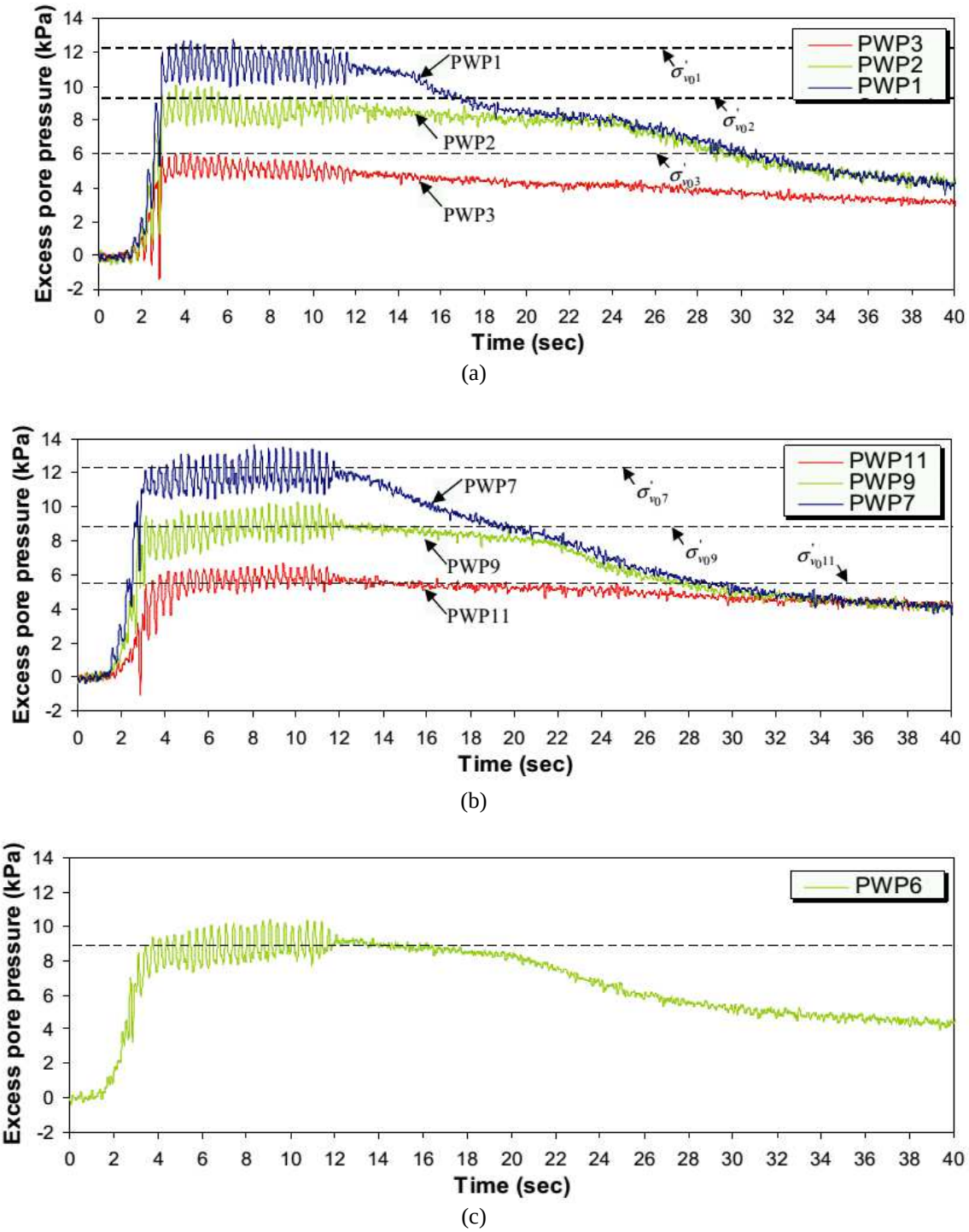

Fig. 4 Representative excess pore water pressure records (a) in free field, (b) close to pile P2 and (c) inside pile group PG2

Pore water pressure time histories adjacent to piles generally show that the soil next to the pile liquefied a little later than that in the free field. Contrary to this, the dissipation of excess pore pressure started sooner adjacent to the piles compared to that in the free field. This late initiation of liquefaction and also early dissipation of excess pore pressures close to the piles can be interpreted by separation of the soil and pile at down-slope side of the pile during lateral soil movement and consequently formation of a drainage path along the pile. Time history of pore water pressure recorded inside the pile group PG2 (Fig. 4-c) illustrates that the soil inside the pile group was

also liquefied later than that in the free field which can be attributed to the effects of confinement induced by the piles.

3.3. Records of lateral displacement of pile caps and free field soil

Fig. 5 displays lateral displacement record of the pile caps along with that of the free field soil (recorded by the displacement transducer (LVDT3) near the ground surface) in which positive values correspond to the downslope movement. As seen in this figure, the movement of the crust soil towards downslope started when the soil was approaching initial liquefaction. The soil movement continued until the end of the shaking, ultimately reaching a maximum value of about 73.7 mm. It should be noted that the maximum lateral ground displacement obtained by analyzing the movies recorded from side of the model during lateral spreading was up to 200 mm and occurred near the mid-height of the liquefied layer. This value is much larger than the maximum displacement measured at the ground surface. This issue will be addressed in more detail in section 4.4.

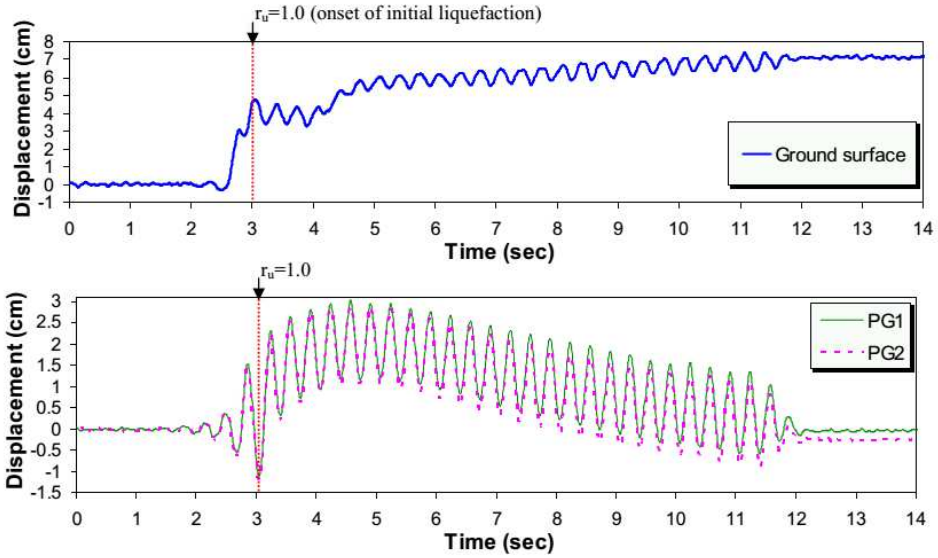

Fig. 5 Time histories of ground surface displacement and lateral displacement of the pile caps

Unlike the free field soil displacement which kept increasing until the end of the shaking, pile cap displacement records show that the pile groups reached the maximum displacement at the caps a few seconds after the occurrence of lateral spreading and then bounced back gradually as the shaking continued, since after the liquefaction, the middle layer was loose enough to allow the pile groups to gradually bounce back due to their rigidity while the liquefied soil was flowing around the piles. The maximum recorded lateral displacements of the pile caps were about 30.0 mm and 28.0 mm in pile groups PG1 and PG2, respectively.

3.4. Pile bending moments

In order to obtain time histories of bending moments, several strain gauges were attached to the piles at predetermined depths which recorded bending strains during the shaking. Half Whetstone bridge configuration was utilized for strain measurements in order to include only bending strains in the records while excluding axial ones. Measured strain data were finally converted to bending moments using Euler-Bernoulli beam theory. Time histories of bending moments in instrumented model piles at some representative depths are displayed in Fig. 6.

The time histories corresponding to deeper depths (close to the base of liquefiable layer) show that bending moments in piles reached the maximum values a few seconds after the beginning of liquefaction and lateral spreading and then decreased gradually with the elastic rebound of the pile groups as described in section 3.3. However, time histories of bending moments at a depth of 20 cm (located in the non-liquefiable crust layer) illustrate that bending moments reached the peak values and remained almost constant until the end of shaking.

It should be noted that as the applied base shaking and the lateral spreading had the same direction, recorded bending moment data consists of cyclic and monotonic components which are respectively due to the inertial and kinematic soil pressures acting on the piles. Inertial soil pressures are exerted by ground oscillations while kinematic pressures are induced by lateral soil flow. Basically, lateral spreading is a post-liquefaction event which includes large monotonic ground displacements. Since the main objective of this paper is to study the effects of lateral spreading, only monotonic components of bending moments are focused on. For this purpose, cyclic component of recorded bending moment data was filtered out by passing the records through a low-pass filter. The monotonic components of bending moments can be observed in Fig. 6, by thick lines.

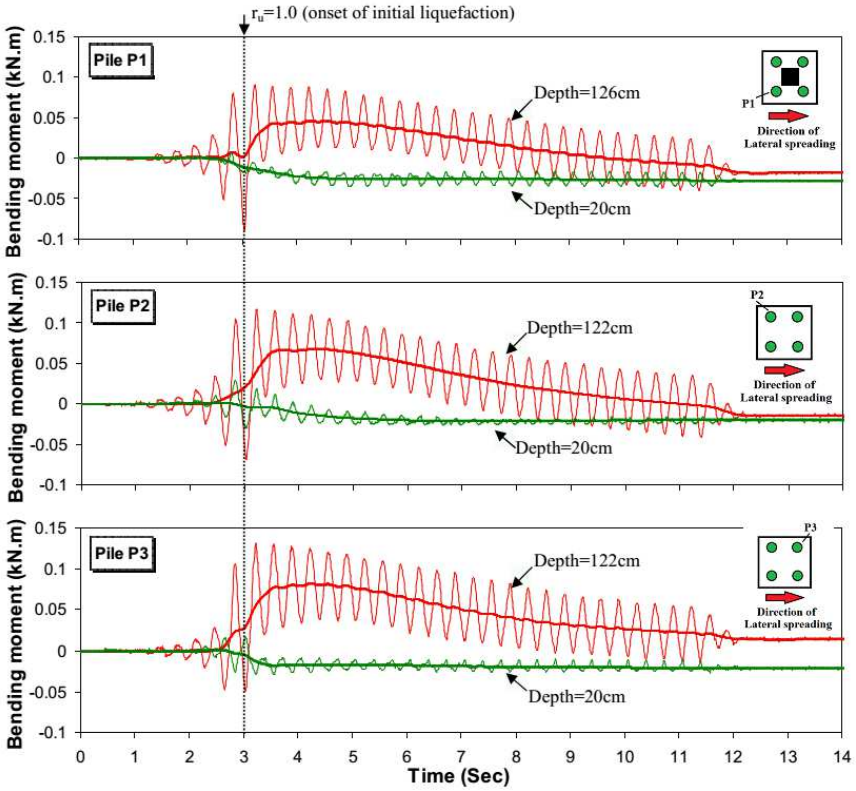

Fig. 6 Bending moment time histories (main data and monotonic components) in instrumented piles at representative depths

Variations of monotonic components of bending moments along the model piles at some time steps of the shaking history are provided in Fig. 7. As seen in this figure, most of the times, sign of bending moments in piles changes at some elevations above the base of liquefied layer. Besides, maximum positive bending moments are observed at the base of liquefied layer while maximum negative bending moments occur at a depth almost close to the middle of liquefied layer. These observations are due to the fact that model piles were fixed against translation and rotation at the base and were partially fixed in the pile cap at the top. In this respect, it should be added that the degree of fixity at the base of the piles was greater than that at the cap, as positive moments at the base are clearly larger than negative ones near the cap. Interestingly, negative bending moments in pile P1 are comparatively larger than those observed for pile P2. These larger bending moments can be attributed to the effects of the mass attached to the pile cap as a superstructure. In this regard, it should be pointed out that the maximum negative bending moment in pile P1 was about 1.4 times that measured in pile P2.

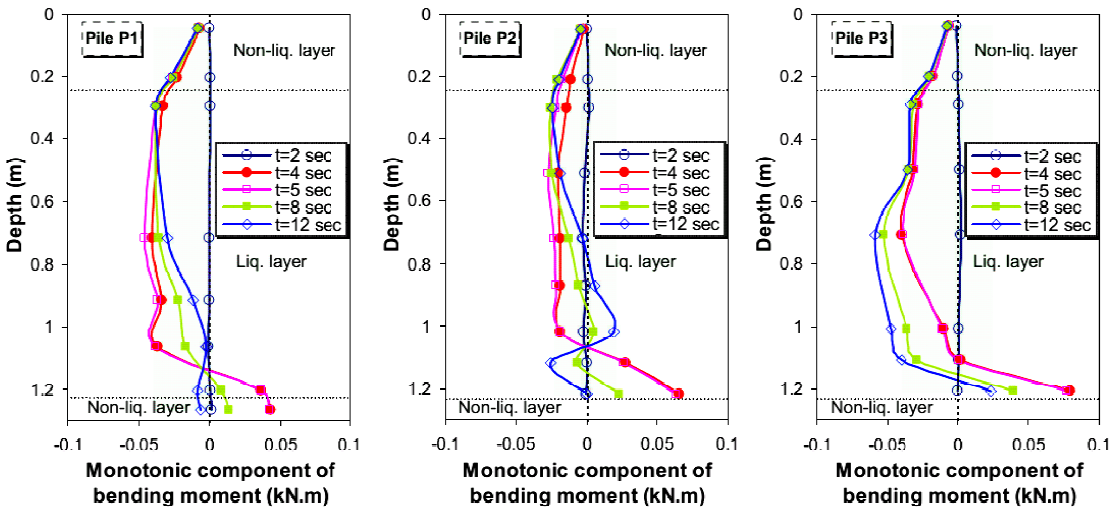

Fig. 7 Longitudinal profiles of monotonic components of bending moments in instrumented model piles

4. Detailed Analysis of Experimental Results

4.1. Lateral force of liquefied soil on the piles

The lateral forces exerted on the individual piles of the groups can be back-calculated from the bending moment distributions, $M(z,t)$, measured along the piles, using the following equation:

$$P(z,t) = \frac{\partial^2 (M(z,t))}{\partial z^2} \quad (1)$$

In this equation, $P(z,t)$ is the lateral force of liquefied soil on the pile due to lateral spreading at depth z and time t. The lateral forces should be determined by double differentiation of bending moment data; however, double differentiation procedure is potentially associated with numerical errors. Different methods have been proposed for reducing such errors to obtain lateral forces from discrete bending moment data points. A common method for such reduction of error is differentiation of polynomial curve fitted to the discrete bending data [28]. However, in this regard, Brandenberg et al. [29] recently proposed a method for error reduction based on minimizing weighted residuals and showed that their proposed method gives better results than conventional procedure of polynomial regression. In this study the method introduced by Brandenberg et al. [29] is implemented for back-calculation of lateral forces of soil from recorded bending moments to minimize the potential numerical errors associated with double differentiation procedure. For determination of lateral forces, monotonic components of recorded bending moments were used in differentiation procedure.

Fig. 8 shows profiles of the monotonic component of lateral forces of liquefied soil back-calculated in this study along with the lateral forces proposed by JRA [27] code for design of pile groups against lateral spreading. This code recommends using 30% of the total overburden pressure to be applied to the outermost width of the pile group as lateral forces due to lateral spreading. In cases with a top non-liquefiable layer, it suggests that the passive pressure from non-liquefiable layer should be considered as well. For design applications, implementing JRA [27], it is commonly assumed that the total lateral force exerted on the pile group is equally distributed among the individual piles of the group.

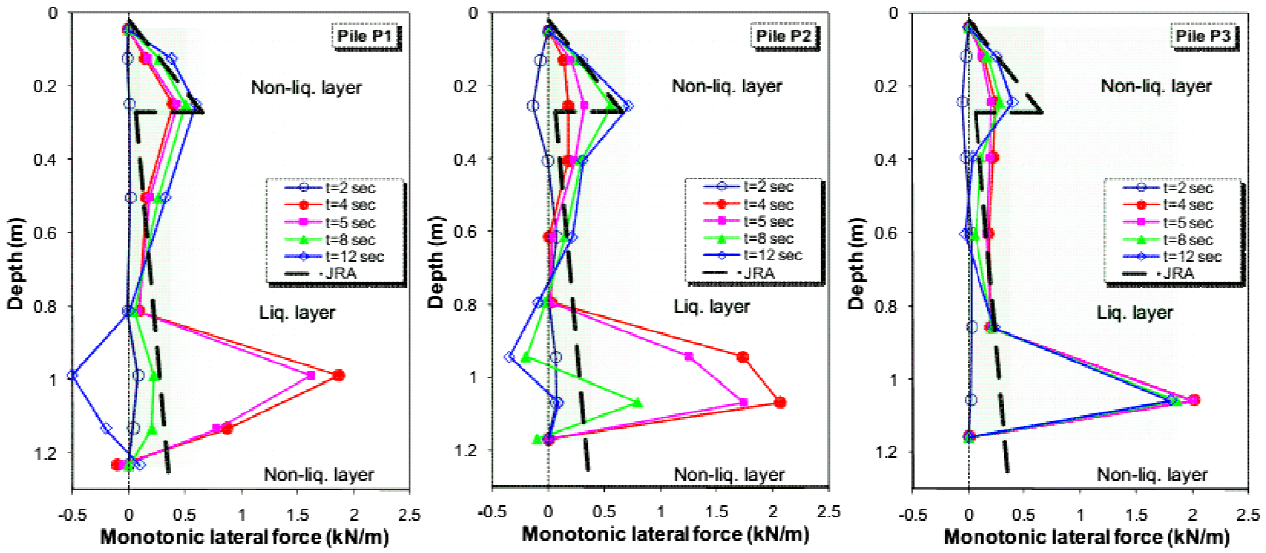

Fig. 8 Profile of monotonic component of lateral forces on individual piles of the groups obtained in this study and those recommended by JRA [27]

As seen in Fig. 8, distribution of exerted lateral forces on all piles follows rather a similar pattern. At the early stages of shaking when the soil was not yet liquefied, induced forces are negligible. But upon liquefaction and following lateral spreading, magnitude of kinematic lateral forces increased significantly. Almost in all diagrams of Fig. 8, an increase in applied lateral forces is observed at upper elevations where the non-liquefiable crust exists. In fact, the non-liquefiable crust layer moved towards the downslope during lateral spreading, exerting extra pressure on the piles. The magnitude of lateral forces from the crust layer was to some extent smaller than the passive pressure suggested by JRA [27] code. In general, in all model piles, back-calculated lateral forces in lower half of the liquefied layer are considerably larger than those obtained at the upper half. Such an observation can be well addressed by larger lateral displacement of the soil in lower half of the liquefied layer when compared to its upper half (as will be shown and discussed later in section 4.4). At the same time, lateral deflections of piles are less in lower elevations resulting in larger relative displacements between soil and pile in such elevations. The agreement between the magnitudes of back-calculated lateral forces with those values recommended by JRA [27] is more in

upper half of the liquefied layer while along the lower half of the liquefied layer, the magnitudes of back-calculated lateral forces are significantly larger than those suggested by JRA [27].

4.2. Total lateral forces exerted on individual piles of the groups

Time-histories of the monotonic components of total lateral forces exerted on the piles were calculated by integrating the lateral soil forces along the piles as given in equation 2. These total lateral forces were separately evaluated for the liquefied layer and the non-liquefiable crust. The calculated time histories are displayed in Fig. 9.

$$F_{L.L_i}(t) = \int_{z=0}^{z=H_1} P_i(z,t)dz$$
$$F_{N.L_i}(t) = \int_{z=0}^{z=H_2} P_i(z,t)dz \quad (2)$$
$$F_i(t) = F_{L.L_i}(t) + F_{N.L_i}(t)$$

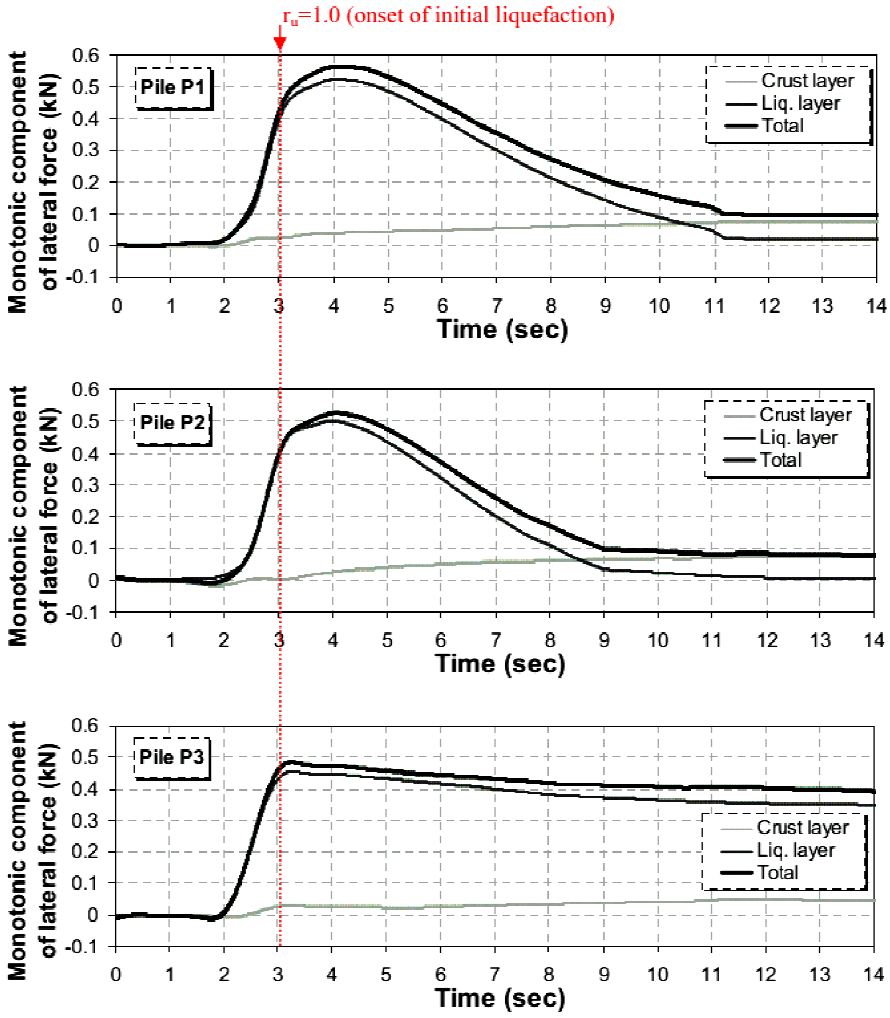

Fig. 9 Time histories of monotonic components of total lateral forces in different piles of the model

In above equations $F_{L.L_i}(t)$ and $F_{N.L_i}(t)$ are time histories of total lateral forces exerted on pile i by the liquefiable layer and non-liquefiable crust, respectively. $F_i(t)$ is time history of the total lateral force exerted on pile i and H_1 and H_2 are the thicknesses of liquefiable layer and non-liquefiable crust, respectively. Fig. 9 demonstrates that total lateral forces increased in early stages of the shaking when liquefaction and lateral spreading occurred, attaining the peak value, and then decreased while the piles were bouncing back showing a residual value at the end of the shaking. However pile P3, as the downslope pile of the group, behaves differently in this respect since the amount of residual force observed in this pile is much larger than those observed in piles P1 and P2, the upslope piles of the two groups of piles. The separation of soil from downslope side of pile P3 during the lateral soil movement can be considered as a reason for such different behavior.

Another worth-noting observation is that the lateral

forces exerted by the crust layer kept increasing during shaking while those exerted by the liquefied layer reached a peak and then decreased indicating the phase difference between the lateral loads exerted by crust and liquefied layer. This fact is graphically shown in Fig. 10 for pile P1 as an example. The reason behind such an observation is the fact that the liquefied soil showed minimum resistance to pile rebound during shaking while the crust layer kept its resistance, exerting additional lateral force on the piles at upper elevations.

In Fig. 11, back-calculated monotonic components of maximum total lateral forces in different individual piles of the groups are compared. The main findings from the comparison can be itemized as below:

- Comparing maximum total lateral force in piles P1 and P2 (arrow 1 in Fig. 11), indicates that the monotonic component of total lateral load exerted on pile P1 is about 1.07 times that exerted on pile P2. This observation can be attributed to the effect of superstructure on the monotonic lateral load exerted on pile P1 during lateral spreading.

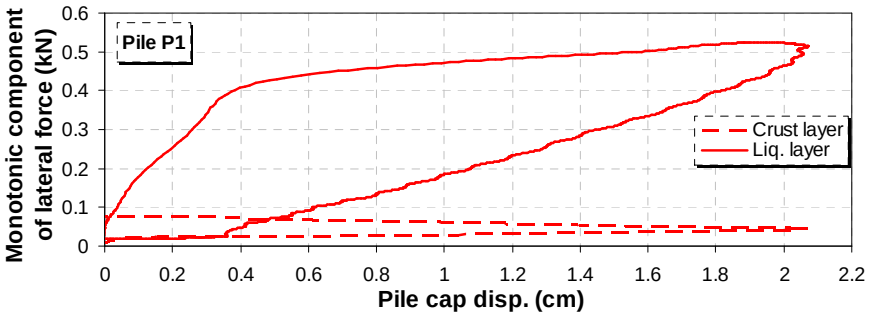

Fig. 10 Variations of lateral forces exerted by crust and liquefiable layers versus pile cap displacement

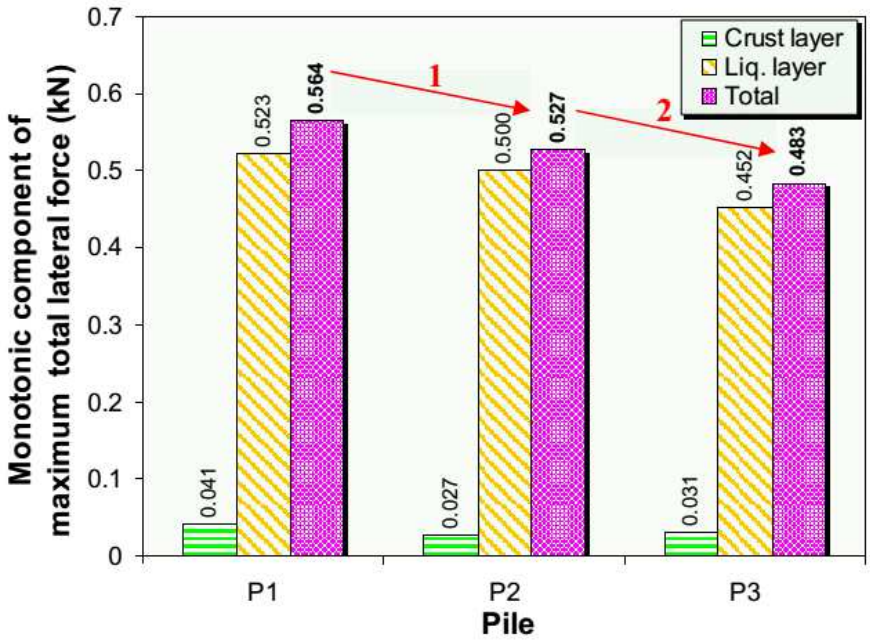

Fig. 11 Comparison between back-calculated monotonic components of maximum total lateral forces in individual piles of the groups

- The amount of total lateral force in pile P2 (the front or upslope pile) is about 1.09 times of that observed for pile P3, the shadow or downslope pile (arrow 2 in Fig. 11). This finding is consistent with the results of a recent study conducted by Haeri et al. [18] on a group of single piles (without cap).

- The shadow effect as described above is only attributed to lateral forces exerted by lateral spreading on piles in liquefiable layer. Ironically, the magnitude of lateral force exerted by the crust layer on pile P3 (shadow pile) is about 15% higher than that exerted on pile P2. This issue can be well described by the separation occurred at the downslope of pile P3 resulting in lack of lateral support from the soil in the crust layer. Concrete evidence for such separation of soil and pile, extracted from a movie recorded from the top of physical model during the experiment, is shown in Fig. 12.

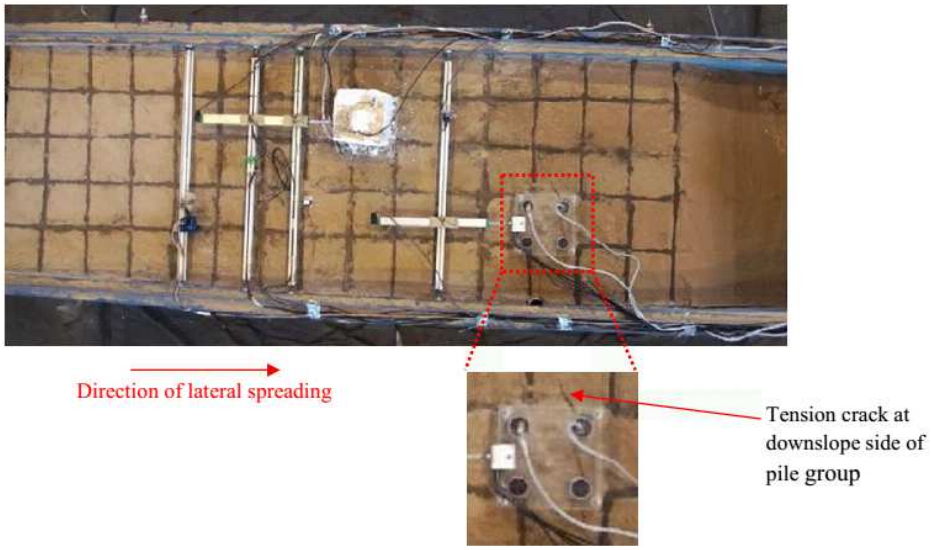

Fig. 12 Separation between soil and downslope pile row (pile group PG2) during lateral spreading (t=4.0 sec)

The photo shown in this figure illustrates the surface of the model at time of about 4.0 sec when development of the first tension crack at downslope side of the pile group PG2 is observed. The tension crack was detectable until the end of shaking, providing evidence for different behavior of pile P3 as previously discussed and shown in Fig. 9.

It should be noted that quantitative comparison between the exerted lateral forces on the piles as discussed above is somewhat preliminary at this stage and needs further experimental investigations to be generalized.

4.3. Total lateral forces exerted on the pile groups

Total lateral forces applied on each rows of the group and subsequently on the whole group can be estimated from Equations 3 and 4, respectively.

$$F_{row_j}(t) = \sum_{i=1}^{2} F_i(t) \tag{3}$$

$$F_{total}(t) = \sum_{j=1}^{2} F_{row_j}(t) \tag{4}$$

In above equations $F_{row_j}(t)$ is time history of total lateral force applied to jth row of piles and $F_{total}(t)$ is time history of total lateral force exerted on the pile group. It should be noted that in current experiment, only one pile in each rows of the groups was instrumented but due to the symmetry it was assumed that both piles in a row receive the same total lateral forces. Total forces exerted on each pile group resulted from this experiment are compared with those recommended by JRA [27] in Fig. 13.

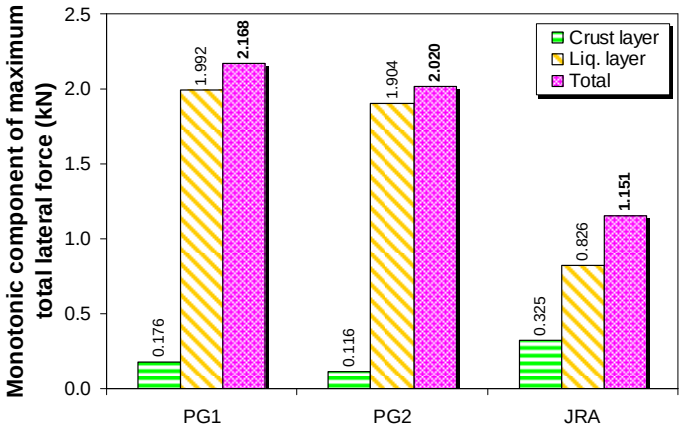

Fig. 13 Comparison between monotonic components of maximum total lateral forces in different pile groups from this experiment and JRA [27] recommended values

Total lateral forces exerted on pile group PG1 which has a lumped mass and pile group PG2 are respectively about 88% and 75% higher than the values calculated using recommendations of JRA [27]. The differences are found to be more profound if only lateral forces from liquefiable layer are compared. This issue has been previously pointed out by other investigators for pile groups located in mild slopes or behind quay walls (e.g., Motamed et al. [16] and Motamed and Towhata [30]). However, the trend observed for the non-liquefiable crust layer is completely different as the lateral forces suggested by JRA [27] is in average about 2.3 times the experimental values observed for pile groups PG1 and PG2. The reason is that passive pressure recommended by JRA [27] for non-liquefiable crust layer is applicable provided that a passive failure wedge is formed in the crust layer while relative displacement between the pile cap and the crust layer in this experiment does not seem to be enough for formation of a failure wedge and development of subsequent passive pressure in the crust layer.

Based on the formula given in Equations 3 and 4,

contributions of each row of piles in total lateral force sustained by the pile group can be evaluated in terms of numerical values called contribution coefficients as:

$$C_{row_j} = \frac{F_{row_j}^{\max}}{F_{total}^{\max}} \quad (5)$$

where $F_{row_j}^{\max}$ is the maximum total lateral force exerted on jth row of piles, $F_{total}^{\max}$ is the maximum total lateral force exerted on the pile group and C_{row_j} is the contribution coefficient of jth row. Contribution coefficients calculated for front (upslope) and rear (downslope) pile rows of the 2×2 pile group (PG2) in this study are depicted in Fig. 14. As seen in this figure, in liquefiable layer, the upslope row of piles carries larger lateral forces than the downslope one while in non-liquefiable crust layer, the downslope row sustains greater forces and in overall, the contribution coefficient of total lateral force in upslope row is greater than that obtained for downslope row.

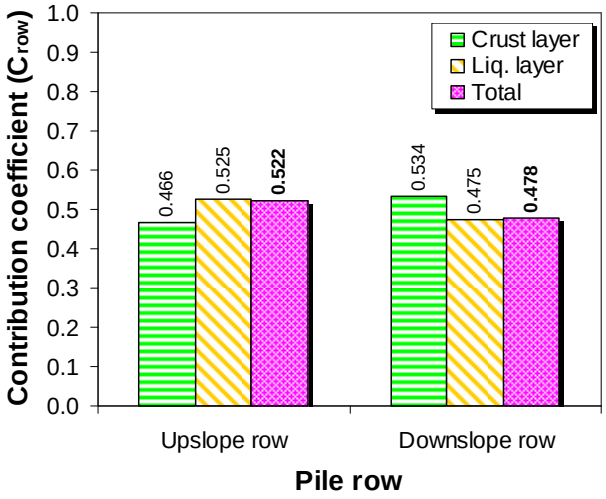

Fig. 14 Contribution coefficients of different pile rows

Motamed and Towhata [30] based on shaking table experiments on 3×3 pile groups in single liquefiable layer behind quay wall, proposed contribution indexes of lateral forces in individual piles of the group depending on their position within the group. The contribution indexes obtained by these investigators increased in longitudinal direction, parallel to the direction of lateral spreading. In other words, those piles located in upslope carried less lateral forces than those located in downslope, near the quay wall. These facts show that the distribution of lateral forces in individual piles of a pile group located in a mild slope, such as the case in current experiment differs from that in a pile group located behind a quay wall as observed by Motamed and Towhata [30]. The main reason for this different behavior is that pattern and magnitude of soil displacements in a mild slope differ from those behind a quay wall.

4.4. Pattern of soil displacement during lateral spreading

In order to monitor the lateral displacement of soil during lateral spreading, digital high speed cameras and camcorders were implemented both at top and side of the model. Colored sands were formed in a grid pattern at surface of the model as well as in vertical columns at side of the model behind the Plexiglas windows. Patterns of soil displacement in vertical cross section view and at surface of the model were obtained by analyzing the photos taken from side of the model and the movies recorded from top of the model, respectively. Fig. 15 shows the profile of lateral soil displacement in free field at selected times during the shaking providing a valuable opportunity for assessing lateral soil movement while lateral spreading occurred. As seen in this figure, the maximum permanent soil displacement is about 20cm at the end of shaking which occurs near the middle of the liquefiable layer. The maximum lateral soil displacement in non-liquefiable crust layer occurs at the ground surface which is considerably smaller than the maximum displacement observed in liquefied layer. Displacement values show a significant reduction near the boundaries between the middle liquefiable layer and upper and lower non-liquefiable layers. This reduction in movement of liquefiable soil can be attributed to the frictional forces exist at the interface of liquefiable and non-liquefiable soils.

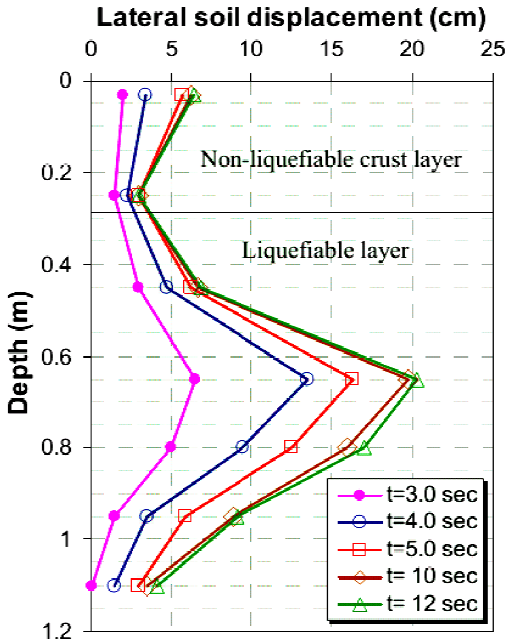

Fig. 15 Profile of lateral soil displacement in free field at upslope side of the model extracted from snapshots during the shaking

A Contour plot showing the lateral displacement of ground surface at the end of shaking is provided in Fig. 16. Since some parts of the ground at downslope of the model were submerged, it was not possible to obtain soil displacements in those areas by analyzing the recorded movies. For this reason, an area located at the downslope, 0.5m far from the end of rigid box is not covered in the contour plot. Fig. 16 demonstrates that the largest soil

displacements are observed at upslope and downslope parts of the ground surface while magnitude of displacement decreases at the vicinity of the pile groups. Significant reduction in soil displacement is also observed at upslope side of the pile groups illustrating that the movement of crust layer was blocked due to the presence of piles.

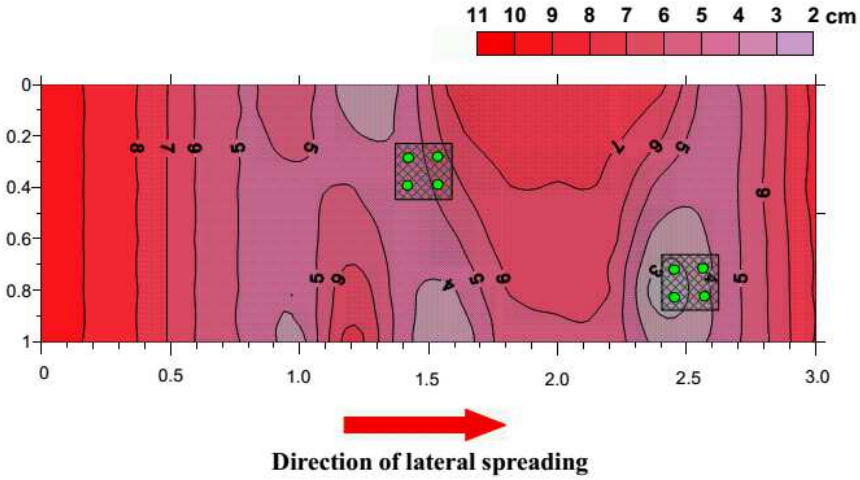

Fig. 16 Contour map of lateral displacement of ground surface at the end of shaking

4.5. Back-calculated p-y curves

A p-y curve correlates the lateral soil pressure with the relative displacement between the soil and the pile which is widely used in practical applications for analytical or numerical analysis of soil-pile interaction.

In order to further investigate the interaction between the pile group and the laterally spreading soil in this study, p-y curves were back-calculated from the experimental data. For this purpose, monotonic soil pressures were obtained by the same procedure previously explained in section 4.1 for obtaining lateral forces and then relative displacements between soil and pile were obtained as:

$$y(z,t) = y_g(z,t) - y_p(z,t)$$
$$y_p(z,t) = \iint \frac{M(z,t)}{EI} d^2z \qquad (6)$$

In above equations, $y(z,t)$ defines time history of relative displacement between soil and pile, $y_g(z,t)$ is time history of displacement of free field soil and $y_p(z,t)$ is time history of displacement in each individual pile, all at depth z. Two boundary conditions are required for evaluation of pile displacements from equation (6) which can be selected as displacements at the base and head of the pile. Displacement at the base of the pile was considered to be zero as the pile was fixed at its base and displacement of the pile head was obtained from the displacement data recorded by the transducer attached to the pile cap. For evaluation of relative displacements, all cyclic components were filtered out. In addition, since the variation of free field soil displacement with time was not digitally measured in depth by electronic sensors and was only known at ground surface (from surface LVDT mounted at free field of the model), the profile of lateral soil displacement was assumed to follow the same pattern obtained by analyzing the side photos as previously shown in Fig. 15.

Back-calculated p-y curves for the instrumented model piles at various depths are provided in Fig. 17. As seen in this figure, p-y curves in all piles and at different depths of liquefied soil generally consist of two rising (hardening) and falling (softening) portions (except those corresponding to the soils close to the boundary of liquefiable and non-liquefiable layers) while p-y curves of non-liquefiable crust only consist of a rising part. This contradictory behavior implies that the crust layer kept its resistance during lateral spreading while the strength of liquefied soil degraded after liquefaction. In other words, the lateral pressure by the non-liquefiable crust kept increasing up to the end of lateral spreading without any evidence of yielding of the soil in the crust layer. This is completely consistent with the trends observed in time histories of lateral forces of crust layer on piles, previously discussed in section 4.2. On the other hand, the lateral pressure induced by the liquefied soil increased to a maximum value that in turn created the maximum deflection in the pile where the rigidity of the pile resisted against additional deflection. At that time, the liquefied soil was not able to withstand the elastic reaction from the pile and consequently the soil failed allowing the pile group to bounce back. After the peak point, the unbalanced lateral pressure by the liquefied layer kept decreasing. It should be added that the soil at depth of 30 cm located in liquefiable layer (adjacent to the crust layer) shows a p-y behavior similar to that observed for the crust.

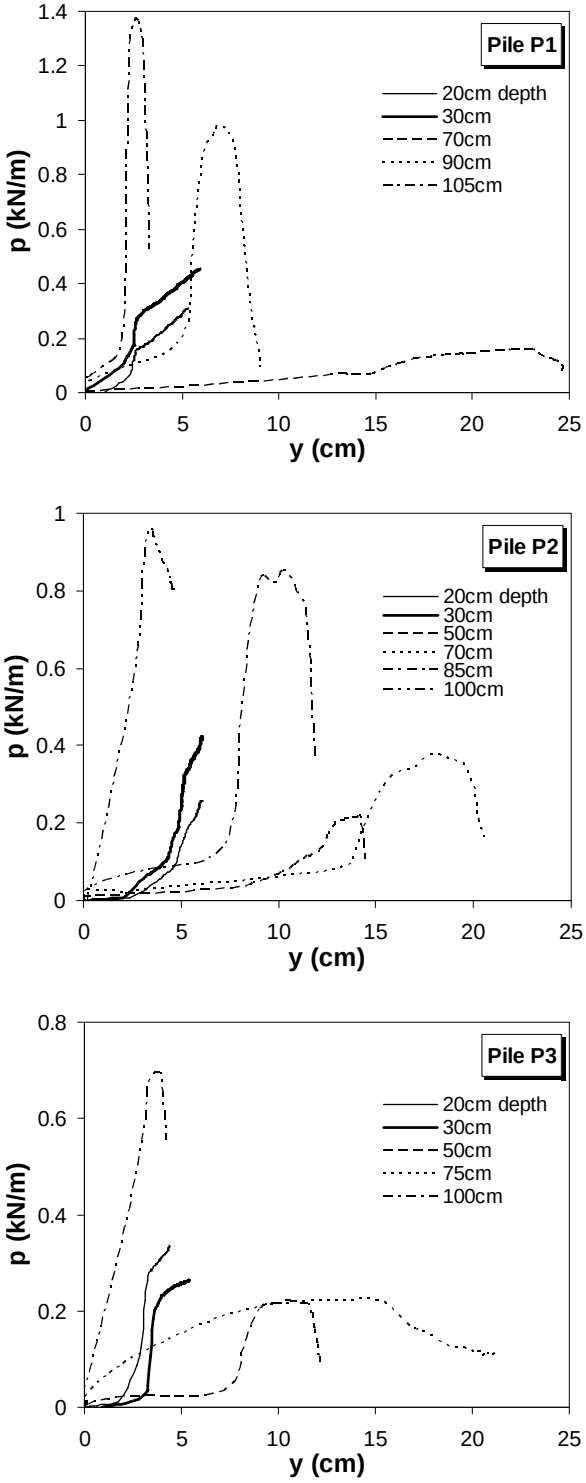

Fig. 17 Back-calculated p-y curves for individual piles of the groups

Almost in all p-y curves of liquefied soil, the maximum lateral resistance and also the maximum initial stiffness of liquefied soil are observed at deeper depths while the minimum values are obtained at shallower depths. Additionally, the ultimate resistance of liquefied soil at deeper depths mobilized in smaller displacements compared to the shallower depths in which the peaks of p-y curves are observed at quite large relative displacements.

It is also interesting to note that in upslope piles of the groups (piles P1 and P2), it is observed that the p-y curves corresponding to depth of 30cm are located above those related to depth of 20cm, almost in entire range of displacements, while for downslope pile (P3), the reverse trend is observed. Such a different behavior can be attributed to the formation of the gap between the soil and the downslope side of pile P3.

5. Observation of Physical Model After Lateral Spreading

Ground surface and also sidewalls of the physical model were carefully examined after the experiment to visually investigate the effects of lateral spreading. Fig. 18 shows a photograph taken from the surface of the model after lateral spreading. As seen, some surficial cracks are detectable in upslope part of the model which are due to the lateral soil movement in addition to the liquefaction-induced settlements.

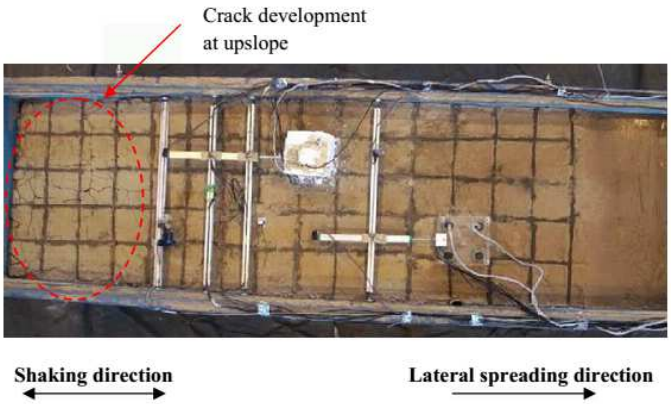

Fig. 18 A photograph of the ground surface after liquefaction and lateral spreading

6. Numerical Analysis of Pile Group Response

6.1. Force based method

Response of pile groups under lateral spreading can be evaluated by the force based method in which the exerted lateral pressures are modeled as imposed limiting pressures similar to the procedure that JRA [27] code recommends. Based on this procedure, the profile of exerted lateral pressure on the pile group can be obtained as:

$$P(h)=\begin{cases} K_p\gamma_{N.L}h & 0\le h\le H_1 \\ 0.3[\gamma_{N.L}H_1+\gamma_{L.L}(h-H_1)] & H_1<h\le H_1+H_2 \end{cases} \quad (7)$$

In above equation $\gamma_{N.L}$ is the unit weight of non-liquefiable crust that is $16.0\,kN/m^3$, $\gamma_{L.L}$ is the saturated unit weight of the liquefiable soil which is equal to $19.5\,kN/m^3$, K_p is the Rankine passive pressure coefficient for crust layer being equal to 3.25 by assuming $\varphi=32^\circ$ as angle of friction of the soil in the crust, H_1 and

H_2 are in turn thicknesses of non-liquefiable crust and liquefiable layers and h is the depth measured from the ground surface. Obtained pressures based on the above procedure (Fig. 19a) were used to conduct a static analysis of the pile groups under lateral spreading implementing SAP2000 [31] software. The pile groups were modeled as plane frames and P-delta effect was considered in the analyses to investigate the effects of superstructure on pile response during lateral spreading. However, it should be kept in mind that inertial loading from superstructure during the shaking is not considered herein. In addition, in order to precisely model the fixity conditions at the base of piles and also at the pile-cap connections, rotational springs were used in these locations. For this purpose, rotational stiffness of the springs at the connections of the piles to the base ($K_{\theta b}$) and the cap ($K_{\theta t}$) are defined as:

$$K_{\theta b} = \frac{M_b}{\theta_b}$$
$$K_{\theta t} = \frac{M_t}{\theta_t} \quad (8)$$

where M_b and M_t are measured bending moments in piles at the connection to the base and the cap, respectively while θ_b and θ_t define the corresponding back-calculated rotations at these locations. Using the experimental data, $K_{\theta b}$ and $K_{\theta t}$ were estimated to be 3.58 and 0.52 kN.m/rad, respectively.

In order to obtain exerted lateral forces and subsequent induced bending moments in individual piles of the group, it was assumed that total lateral force exerted on the pile group is equally shared among the individual piles.

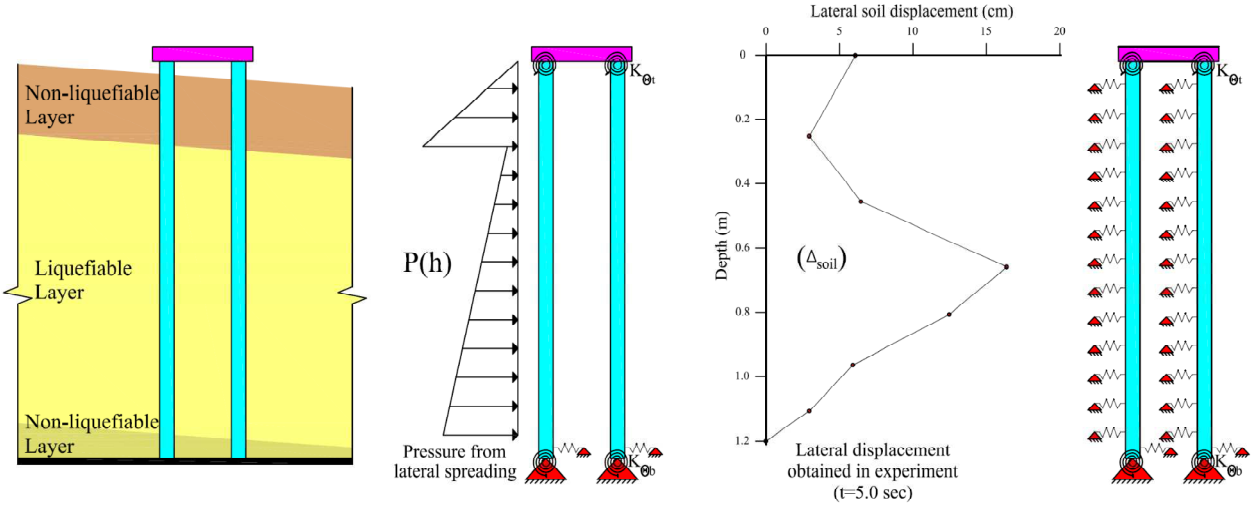

Fig. 19 Numerical analysis of pile groups under lateral spreading (a) force based method, (b) displacement based method

6.2. Displacement based method

Another widely accepted procedure for the analysis of pile groups under lateral spreading is the displacement based approach in which a Beam on Nonlinear Winkler Foundation (BNWF) model is utilized. As depicted in Fig. 19(b), in this approach profile of free-field lateral soil displacement (Δ_{soil}) is applied at free ends of the p-y springs of laterally spreading soil. A wide range of empirical models are available for determination of free-field lateral soil displacement (e.g. Baziar and Saeedi Azizkandi [32], among others). However, most of these models are only capable to predict lateral displacement of the ground surface; therefore for practical applications, the variation of ground displacement with depth should be evaluated by simple approximations. In this study, the input free-field soil displacement in calculations was selected to be equal to that measured in the experiment, as previously depicted in Fig. 15. It should be added that the displacement based method is essentially a pseudo-static analysis by which the maximum bending moment is evaluated for design purposes. Thus the profile of soil displacement utilized in this method should be specified at the same time that the maximum bending moment is observed in the pile which is about $t = 0.5$ sec in current experiment.

In order to obtain the p-y curve for a liquefied or laterally spreading soil, a reduction factor, known as p-multiplier is usually applied to the corresponding p-y curve of the non-liquefied soil. In this respect, design diagrams have been proposed by different researchers or codes of practice, most of them correlating p-multipliers with $(N_1)_{60}$ values, among which those introduced by Brandenberg [33] and Architectural Institute of Japan (AIJ) [34] can be pointed out as the most popular ones. The most commonly used p-y curves in lateral pile design applications are those introduced by API [35]. In this study, standard p-y curves recommended by API [35] for non-liquefiable soil were multiplied by the appropriate reduction factors to obtain the corresponding curves for laterally spreading soil. For this purpose, the value of SPT blow count (N_{SPT}) was assumed to be $(N_1)_{60}$=12 for D_r=40% of the liquefiable soil layer of this study and consequently the reduction factors were estimated to be

0.113 and 0.190 using the average values proposed by Brandenberg [33] and AIJ [34]. It should be added that, for those depths located in non-liquefiable crust layer, no reduction factor was applied to the p-y curves. Obtained p-y curves as discussed above were ultimately used to specify the parameters needed for nonlinear static analysis of the pile groups subjected to lateral spreading using SAP2000 [31].

6.3. Numerical results and discussion

The pile groups of this study were analyzed under lateral spreading by two common methods used in practice, namely force based and displacement based methods. In order to evaluate the capability of these two methods in predicting the behavior of pile groups of this study, profiles of bending moment in different model piles were calculated based on each method and the results are provided in Fig. 20. Note that the p-multiplier values used in the calculations are the average values proposed by Brandenberg [33] and AIJ [34]. Referring to Fig. 20, it appears that the displacement based method using the average p-multiplier value proposed by Brandenberg [33] outperforms all the other methods in predicting the induced bending moments in different model piles especially in depths less than 0.8m. In this regard, the consistency of measured and calculated bending moments using this method seems to be more for piles P2 and P3 than pile P1 (the individual pile of a group with superstructure). Besides, this method predicts the maximum negative bending moments, occurring close to the middle depth of the model, reasonably well in all model piles; while the estimated maximum positive bending moments which occur at the base of the piles are far larger than those recorded during the experiment. This could be due to the fixity conditions at the base of the piles employed in the analyses which might be slightly different from those existed in the experiment.

The displacement based method with average p-multiplier value of AIJ [34] overpredicts both positive and negative bending moments. However, using a p-multiplier value of about 0.110 which is read from the lower bound curve of AIJ [34] will significantly improve the agreement between the computed and recorded data.

It can also be observed in Fig. 20 that the force based approach based on JRA [27] loading, underpredicts the maximum negative bending moments in the piles while overpredicting the maximum positive ones. In fact, the general shape of bending moment profile predicted by using lateral load pattern of JRA [27] is not consistent with the shape of that measured in the experiment. In general, it can be mentioned that the force based method which uses JRA [27] recommended loading is not able to predict satisfactorily the bending moment profile recorded in current experiment. One reason can be the fact that in force based approach, no information regarding the magnitude and pattern of lateral soil displacement profile is considered in the analysis. This can be mentioned as one of the drawbacks of using force based approach for predicting the response of pile groups under lateral spreading.

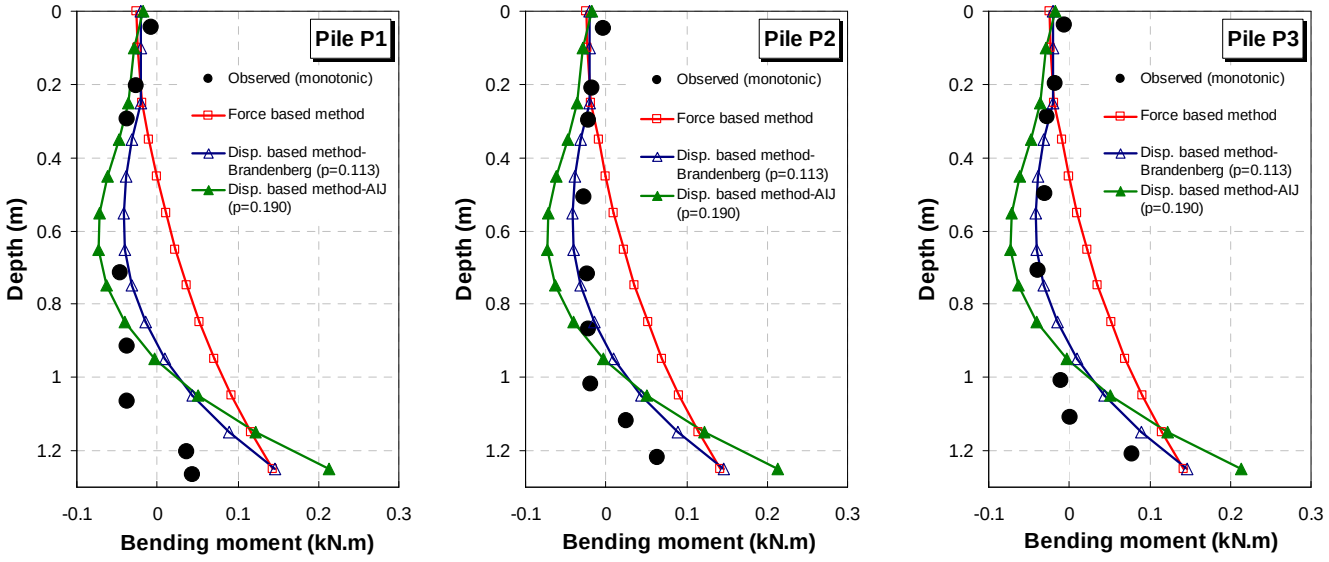

Fig. 20 Comparison between measured and computed bending moments along the model piles

In general, based on the results of numerical analyses, it can be concluded that displacement based approach is more capable of predicting the pile group behavior under lateral spreading. However, it should be kept in mind that as the results of this study illustrate, predicted bending moments by displacement based method highly depend on p-multiplier values or the stiffness of p-y springs adopted in the analysis. Also the degree of fixity (at the base and the cap) considered in the numerical model plays an important role in this regard. Therefore, proper evaluation of these parameters is crucial when adopting displacement based method using p-y springs.

Moreover, as the results of this research show, the response of an individual pile in a group varies based on the pile position within the group while in ordinary displacement based approach this issue is not taken into account. As a result, it is recommended that while using displacement based method in practical applications,

p-multiplier values be adjusted in an appropriate way to accommodate the effects of pile position in the group. Otherwise, it would be wise to use this method just for obtaining an average estimation of the response of individual piles of a pile group.

7. Summary and Conclusions

The behavior of 2×2 pile groups embedded in a 3-layer soil profile consisting of a base non-liquefiable layer, a middle liquefiable layer and a crust non-liquefiable layer, was investigated by conducting 1g large scale shake table test. Experimental results regarding the response of free field soil (e.g. acceleration, pore water pressure and lateral displacement) and piles (e,g. bending moment and lateral cap displacement) were presented and explained in the paper. Lateral soil pressures on model piles were back-calculated from the bending moment data and used to obtain the distribution of lateral forces among the individual piles of the groups. Additionally, numerical analyses using p-y curves were carried out to predict the response of model piles during lateral spreading. The main findings of this research can be summarized as below:

1. Records of lateral displacements associated with lateral spreading indicate that unlike the free field lateral soil displacement which kept increasing until the end of shaking, the pile groups at the caps reached the maximum displacement a few seconds after the occurrence of the lateral spreading and then bounced back gradually as the shaking continued.

2. In all model piles, maximum positive bending moments are observed at the base of the liquefied layer while maximum negative bending moments occur at a depth almost close to the middle of liquefied layer. The presence of superstructure was found to intensify the negative bending moments in the piles.

3. In this experiment (2x2 pile groups), the magnitudes of back-calculated lateral forces due to lateral spreading on piles are significantly larger than those suggested by JRA [27] code at the lower half of the liquefiable layer which consists of medium dense sand.

4. Based on the calculated contribution coefficients of lateral forces, in liquefiable layer, the upslope row of the piles carried larger lateral forces than the downslope one while in non-liquefiable crust layer, the downslope row experienced greater forces. However, contribution coefficient of total lateral force in upslope row was in overall greater than that obtained for downslope row.

5. The maximum lateral soil displacement in a vertical cross section of the model is observed near the middle of the medium dense liquefied layer while displacement values show a significant reduction near the boundaries between the middle liquefied layer and upper and lower non-liquefiable layers. The largest ground surface displacements are observed at free field parts of the model while the magnitude of displacement decreases at the vicinity of the piles. Significant reduction in ground surface displacement is observed at upslope side of the pile groups since the movement of crust layer was blocked by the pile groups.

6. Back-calculated p-y curves in all model piles and at different depths of liquefied soil consist of two rising (hardening) and falling (softening) portions (except those corresponding to the soils close to the boundary of liquefiable and non-liquefiable layers) while p-y curves of non-liquefiable crust only consist of a rising part.

7. Based on the results of a numerical analysis of this experiment it is concluded that the displacement based approach is more capable to predict the behavior of pile groups under lateral spreading. However, proper selection of different mechanical parameters of the numerical model is vital when adopting displacement based method using p-y springs.

Acknowledgments: This study was conducted as part of the research contract number 88B8T1P10 (STR), between Sharif University of Technology (SUT) and Transportation Research Institute, Ministry of Road and Urban Development of Iran. The experiment was conducted using Shake Table Facilities of Earthquake Engineering Research Center, Civil Engineering Department, Sharif University of Technology.

References

[1] Hamada M, Yasuda S, Isoyama R, Emoto K. Study on liquefaction induced permanent ground displacements, Association for the Development of Earthquake Prediction, Japan, 1986.

[2] Hamada M, Isoyama R, Wakamatsu K. Liquefaction induced ground displacement and its related damage to lifeline facilities, Soils and Foundations, January (Special Issue), 1996, pp. 81–97.

[3] Bardet JP, Kapuskar M. Liquefaction sand boils in San Francisco during 1989 Loma Prieta earthquake, Journal of Geotechnical and Geoenvironmental Engineering, 1993, No. 3, Vol. 119, pp. 543-562.

[4] Tokimatsu K, Mizuno H, Kakurai M. Building damage associated with geotechnical problems, Soils and Foundations, January (Special Issue), 1996, pp. 219-234.

[5] Tokimatsu K, Asaka Y. Effects of liquefaction-induced ground displacements on pile performance in the 1995 Hyogoken–Nambu earthquake, Special Issue of Soils and Foundations, 1988, pp. 163-177.

[6] Eberhard M, Baldridge S, Marshal J, Monney W, Rix J. The Mw 7.0 Haiti earthquake of January 12, USGS/EERI Advance Reconnaissance Team, Team report, February 23, 2010, Vol. 1.1.

[7] Abdoun T, Dobry R. Evaluation of pile foundation response to lateral spreading, Soil Dynamics and Earthquake Engineering, 2002, Vol. 22, pp. 1051–1058.

[8] Tokimatsu K. Performance of pile foundations in laterally spreading soils, Proceedings of the Second International Conference on Earthquake Geotechnical Engineering, 1999, Vol. 3, pp. 64–957.

[9] Hamada M. Performance of foundations against liquefaction-induced permanent ground displacement, Proceedings of the 12th World Conference on Earthquake Engineering, Auckland, New Zealand, Paper No. 1754, 2000.

[10] Tokimatsu K, Suzuki H, Sato M. Effects of inertial and kinematic interaction on seismic behavior of pile with embedded foundation, Soil Dynamics and Earthquake Engineering, 2005, Vol. 25, pp. 753-762.

[11] Cubrinovski M, Kokusho T, Ishihara K. Interpretation from large-scale shaking table tests on piles undergoing lateral spreading in liquefied soils, Soil Dynamics and Earthquake Engineering, 2006, Vol. 26, pp. 275-86.

[12] Dungca JR, Kuwanoa J, Takahashib A, Saruwataria T, Izawaa J, Suzukic H, Tokimatsu K. Shaking table tests on the lateral response of a pile buried in liquefied sand, Soil Dynamics and Earthquake Engineering, 2006, Vol. 26, pp. 287-295.

[13] Towhata I, Sesov V, Motamed R, Gonzales M. Model tests on lateral earth pressure on large group pile exerted by horizontal displacement of liquefied sandy ground, Proceedings of the 8th U.S. National Conference on Earthquake Engineering, 2006, April 18–22, San Francisco, California, Paper No. 1227.

[14] He L, Elgamal A, Abdoun T, Abe A, Dobry R, Hamada M, Menses J, Sato M, Shantz T, Tokimatsu K. Liquefaction-induced lateral load on pile in a medium Dr sand layer, Journal of Earthquake Engineering, 2009, No. 7, Vol. 13, pp. 916-938.

[15] Motamed R, Towhata I, Honda T, Yasuda S, Tabata K, Nakazawa H. Behavior of pile group behind a sheet pile quay wall subjected to liquefaction-induced large ground deformation observed in shaking test in E-DEFENCE project, Soils and Foundations, 2009, No. 3, Vol. 49, pp. 459-475.

[16] Motamed R, Sesov V, Towhata I, Anh NT. Experimental modeling of large pile groups in sloping ground subjected to liquefaction-induced lateral flow: 1-G shaking table tests, Soils and Foundations, 2010, No. 2, Vol. 50, pp. 261-280.

[17] Dobry R, Thevanayagam S, Medina C, Bethapudi R, Elgamal A, Bennett V, Abdoun T, Zeghal M, El Shamy U, Mercado VM. Mechanics of lateral spreading observed in a full-scale shake test, Journal of Geotechnical and Geoenvironmental Engineering, 2011, No. 2, Vol. 137, pp. 115-129.

[18] Haeri SM, Kavand A, Rahmani I, Torabi H. Response of a group of piles to liquefaction-induced lateral spreading by large scale shake table testing, Soil Dynamics and Earthquake Engineering, 2012, Vol. 38, pp. 25-45.

[19] Haigh SK, Madabhushi SPG. Centrifuge modelling of lateral spreading past pile foundations, Proceedings of the International Conference on Physical Modelling in Geotechnics, St John's, Newfoundland, Canada, 2002.

[20] Abdoun T, Dobry R, O'Rourke T, Goh SH. Pile response to lateral spreads: centrifuge modeling, Journal of Geotechnical and Geoenvironmental Engineering, 2003, No. 10, Vol. 129, pp. 869-878.

[21] Imamura S, Hagiwara T, Tsukamoto Y, Ishihara K. Response of pile groups against seismically induced lateral flow in centrifuge model tests, Soils and Foundations, 2004, No. 3, Vol. 44, pp. 39–55.

[22] Brandenberg S, Boulanger R, Kutter B, Chang D. Behaviour of pile foundations in laterally spreading ground during centrifuge test, Journal of Geotechnical and Geoenvironmental Engineering, 2005, No. 11, Vol. 131, pp. 1378-1391.

[23] Gonzalez L, Abdoun T, Dobry R. Effect of soil permeability on centrifuge modeling of pile response to lateral spreading, Journal of Geotechnical and Geoenvironmental Engineering, 2009, No. 1, Vol. 35, pp. 62-73.

[24] Ashford SA, Juirnarongrit T, Sugano T, Hamada M. Soil–pile response to blast-induced lateral spreading. I: field test, Journal of Geotechnical and Geoenvironmental Engineering, 2006, No. 2, Vol. 132, pp. 152–162.

[25] Iai S, Tobita T, Nakahara T. Generalized scaling relations for dynamic centrifuge tests, Geotechnique, 2005, No. 5, Vol. 55, pp. 355-362.

[26] Iai S. Similitude for shaking table tests on soil–structure–fluid model in 1g gravitational field, Soils and Foundations, 1989, No. 1, Vol. 29, pp. 105–118.

[27] JRA, Seismic design specifications for highway bridges, Japan Road Association, English version, Prepared by Public Works Research Institute (PWRI) and Ministry of Land, Infrastructure and Transport, Tokyo, Japan, 2002.

[28] Towhata I. Geotechnical Earthquake Engineering, Springer, 2008.

[29] Brandenberg SJ, Wilson DW, Rashid MM. Weighted residual numerical differentiation algorithm applied to experimental bending moment data, Journal of Geotechnical and Geoenvironmental Engineering, 2010, No. 6, Vol. 136, pp. 854-863.

[30] Motamed R, Towhata I. Shaking table model tests on pile groups behind quay walls subjected to lateral spreading, Journal of Geotechnical and Geoenvironmental Engineering, 2010, No. 3, Vol. 136, pp. 477-489.

[31] SAP2000-Ver 11.0.4-CSI, Integrated software for structural analysis and design, Berkeley, CA, USA, Computers and Structures Inc, 2004.

[32] Baziar MH, Saeedi Azizkandi A. Evaluation of lateral spreading utilizing artificial neural network and genetic programming, International Journal of Civil Engineering, 2013, No. 2, Vol. 11, pp. 100-111.

[33] Brandenberg SJ. Behavior of pile foundations in liquefied and laterally spreading ground, PhD thesis, University of California at Davis, CA, 2005.

[34] Architectural Institute of Japan (AIJ), Recommendations for design of building foundations, in Japanese, 2001.

[35] API RP 2A-WSD, Recommended Practice for Planning, Design and Constructing Fixed Offshore Platforms, 20th Ed, Washington, DC, 2000.